Preprints.org

Article

Dendrimer Platforms for Targeted Doxorubicin Delivery – Physicochemical Properties in Context to Biological Responses

Magdalena Szota , Urszula Szwedowicz , Nina Rembiałkowska , Anna Janicka-Kłos , Daniel Doveiko , Yu Chen , Julita Kulbacka , Barbara Jachimska *

Article

Dendrimer Platforms for Targeted Doxorubicin Delivery – Physicochemical Properties in Context to Biological Responses

Magdalena Szota [1], Urszula Szwedowicz [2], Nina Rembiałkowska [2], Anna Janicka-Kłos [3], Daniel Doveiko [4], Yu Chen [4], Julita Kulbacka [2] and Barbara Jachimska [1,*]

[1] Jerzy Haber Institute of Catalysis and Surface Chemistry Polish Academy of Sciences, Cracow, Poland
[2] Department of Molecular and Cellular Biology, Faculty of Pharmacy, Wroclaw Medical University, Wroclaw, Poland
[3] Department of Basic Chemistry, Wroclaw Medical University, Wroclaw, Poland
[4] Department of Physics, University of Strathclyde, Glasgow G4 0NG, United Kingdom
[*] Correspondence barbara.jachimska@ikifp.edu.pl; Tel.:+48124251923

Abstract: The unique structure of poly(amidoamine) (PAMAM) dendrimers allows the drug to be enclosed in internal spaces or immobilized on the surface. In the conducted research, the conditions for the formation of the active G4.0 PAMAM complex with doxorubicin hydrochloride (DOX) were optimized. The physicochemical properties of the system were monitored using Dynamic Light Scattering, Circular Dichroism and Fluorescence Spectroscopy. The Quartz Crystal Microbalance with Dissipation Monitoring was chosen to determine the preferential conditions for the complex formation. The highest binding efficiency of the drug to the cationic dendrimer was observed under basic conditions when the DOX molecule was deprotonated. The decrease in the zeta potential of the complex confirms that DOX immobilizes through electrostatic interaction with the carrier's surface amine groups. The binding constants were determined from the fluorescence quenching of the DOX molecule in the presence of G4.0 PAMAM. The two-fold way of binding doxorubicin in the structure of dendrimers was visible in the Isothermal Titration Calorimetry isotherm. Fluorescence spectra and release curves identified the reversible binding of DOX to the nanocarrier. Among the selected cancer cells, the most promising anticancer activity of G4.0-DOX was observed in A375 malignant melanoma cells. Moreover, the preferred intracellular location of the complexes concerning the free drug was found, which is essential from a therapeutic point of view.

Keywords: PAMAM dendrimers; doxorubicin; dendrimer-doxorubicin interactions; drug delivery systems; DDS

1. Introduction

Doxorubicin hydrochloride (DOX) is classified as an anthracycline antibiotic with anticancer properties. Due to its high cytotoxicity, it is widely used as an effective chemotherapeutic agent [1,2]. However, it is also characterized by side effects such as high cardiotoxicity, poor bioavailability, or a tendency to form fibrillar structures under physiological conditions [3,4]. Doxorubicin's self-aggregation behavior may be responsible for its cytotoxicity, multidrug resistance, and reduced anticancer activity. In addition, non-spherical fibrillar aggregates of DOX may impede permeation through bilayers such as cell membranes [4,5]. The aggregation of doxorubicin is favored by its amphiphilic nature due to its structure in both the hydrophilic part of daunosamine and the hydrophobic part of anthracycline [5]. Environmental factors such as pH, temperature, ionic strength, or concentration may also contribute to the aggregation of small drug molecules [4,6]. DOX nanocarriers are being developed to improve their stability and reduce toxicity, particularly cardiotoxicity [7,8]. Currently, the most effective doxorubicin delivery systems are based on

liposomal nanocarriers. One such formulation is based on pegylated liposomal doxorubicin (Doxil® or Caelyx® according to the European trademark) [9], which was approved by the FDA in 1995, and is widely used in oncology, demonstrating similar or higher efficacy compared to conventional doxorubicin [10]. The second, liposomal doxorubicin (Myocet®), was approved in Europe and Canada in 2000, and the FDA granted it "Fast Track" status as a first-line therapy for the treatment of HER2-positive metastatic breast cancer [11]. Liposomal forms of doxorubicin have lower maximum plasma concentrations and longer circulation times than conventional drugs. The circulation time in the bloodstream of free doxorubicin is 0.2h. Encapsulating it in liposomal formulations extends this time to 2-3h, while in pegylated liposomal formulations, up to 55h [12]. Despite its higher therapeutic index and longer circulation time compared to conventional DOX, therapy with pegylated liposomal doxorubicin often cause dose-related toxicities such as mucositis and skin toxicities. Dermal toxicities are not observed with Myocet and are therefore thought to be related to the PEG surface coating. On the other hand, liposomal DOX did not provide long-term stability in the bloodstream [12]. Other challenges associated with liposomal DOX carriers include a lack of efficacy against cancers exhibiting multidrug resistance and accompanying therapy sides effects, such as hypersensitivity or peripheral neuropathy [13,14]. Given the limitations of both free doxorubicin and its commercially available nanocarrier formulations, therapies that can improve its stability and minimize side effects are still being sought.

Poly(amidoamine) dendrimers (PAMAM) are a group of synthetic polymers with a monodisperse nature and nanometer size. They differ from classical linear polymers by their high structural symmetry, branching of functional groups, and surface polyvalency [15,16]. Expanding the structure with additional layers of functional groups leads to higher generations of dendrimers with larger sizes and numbers of functional groups. Due to their structural diversity, dendrimers are widely used in drug or gene delivery and biosensing [17]. Their hydrophobic interior can promote the encapsulation process of active substances, while their numerous end groups immobilize them on the surface [16,18]. Dendrimers of the 4th generation (G4.0 PAMAM) are one of the most extensively studied in the literature for drug delivery due to their non-toxicity and high drug retention capacity, compared to higher generation dendrimers [19,20]. G4.0 PAMAM is a small nanoparticle with a molar mass of 14 kDa and hydrodynamic and gyration radii of R_H= 2.45 ± 0.05 nm and R_g= 1.87 ± 0.02 nm, respectively [21]. Because of its properties, the G4.0 PAMAM dendrimer can bind ligands efficiently and diffuse through the brain parenchyma, thereby crossing the blood-brain barrier (BBB) [20,22]. The contribution of dendrimers in nanoformulations undergoing clinical trials highlights their potential in the pharmaceutical industry. The current pioneer in the pharmaceutical market is Starpharma company, which uses its patented dendrimer-based technology in two different ways: as stand-alone therapeutics (SPL7013/VivaGel®) or through the use of a dendrimer scaffold (Dendrimer Enhanced Product, DEP®) for drug delivery [23]. DEP® with covalently attached drug molecules are designed to improve the activity of anticancer drugs such as docetaxel, cabazitaxel or irinotecan. These DEP®-drug conjugates are in phase II clinical trials [24]. Other examples of dendrimer-based nanodrugs include an anticancer drug conjugate with a PEGylated poly(lysine) dendrimer for the treatment of hematologic and solid tumors (phase I clinical trials) or the G4.0 PAMAM dendrimer N-acetyl-cysteine for the treatment of Covid-19 disease (phase II clinical trials) [25].

From the application point of view, it is worth highlighting the importance of controlling significant drug parameters such as concentration and pH in the potential self-aggregation process of doxorubicin when designing nanosystems. Encapsulation of doxorubicin in nanoparticles could improve the chemical stability of doxorubicin and prevent its degradation. Yoncheva et al. showed that encapsulation of DOX in chitosan-alginate nanoparticles increased its stability and prevented degradation during exposure to light [26]. A similar phenomenon was observed by Bandak et al. for doxorubicin encapsulation in liposomes, which reduced its photodegradation compared to the free drug [27]. Encapsulation in dendrimer nanoparticles can also prevent the degradation of unstable, pH- or light-sensitive drugs [28].

The novelty of the present study is to investigate the effect of doxorubicin deprotonation under alkaline conditions on the interactions with the G4.0 PAMAM dendrimer and verify the performance of the designed nanosystem *in vitro.* UV-vis spectroscopy monitored the stability and partial degradation of DOX under basic conditions. This study focused on analyzing the strength of the drug from the perspective of the concentration and pH-dependent self-aggregation of DOX in aqueous media. Dynamic light scattering (DLS) confirmed the strong effect of pH on the aggregation of drug particles. The concentration-dependent effect of DOX aggregation was depicted using circular dichroism (CD) and fluorescence spectroscopy. The change in the zeta potential of the aggregated forms of doxorubicin as a function of pH was determined. The Quartz Crystal Microbalance with Dissipation Monitoring (QCM-D) was used to form G4.0 PAMAM/DOX bilayers on the gold sensor, thus determining the most effective conditions for DOX binding to the G4.0 PAMAM structure. Depending on pH and drug concentration, the viscoelastic character of the formed layers was determined. Fluorescence Spectroscopy determines the values of the binding constant. The Isothermal calorimetry (ITC) method indicated that DOX undergoes binding to the structure of G4.0 PAMAM in the endothermic process, localizing to two different types of active sites. In vitro tests for G4.0 PAMAM/DOX systems showed that the G4.0 PAMAM dendrimer can be a promising and selective nanocarrier for doxorubicin. The type of cancer cells strongly influences the efficiency of the formed complexes.

2. Results

2.1. Stability and Self-Aggregation of Doxorubicin under Alkaline Conditions

Since the PAMAM dendrimer efficiently binds doxorubicin under alkaline conditions (pH > 8.5) [29], the stability of the free drug was checked under this environment. UV-vis spectroscopy monitored the spectral changes of doxorubicin in relation to pH (pH=8.5, 9.0, 10.0) at 72h (Figure SM1). It was shown that the tendency of changes in the position of spectra and absorbance values strongly depends on the pH of the initial solution. In the case of the solution at pH=8.5, the trend of changes shows no significant effect on the doxorubicin form. The spectrum at pH=8.5 shifts slightly toward higher wavelengths while it returns to the initial state after time. Absorbance increases with time and, after 2 hours, is close to the native solution. The final pH of the doxorubicin solution remains at pH=6.6 and is already constant after 1.5h. A slower pH decrease with time was observed at pH=9.0. The spectrum shifts slightly toward higher wavelengths, and the absorbance decreases relative to the native solution. A reduction in pH over time is observed, but at a slower rate than in the case of a solution with pH=10. The trend of changes in the absorbance over time is different from that of the other solutions. For the first 2.5h, its value increases, indicating the gradual return of the doxorubicin molecule to its initial form, while after this time, it begins to decrease gradually. Finally, after 24h, the solution reaches a constant pH of pH=7.07, while the absorbance is much lower than for the initial form at native pH. The most significant changes are observed for a solution at pH=10. The spectrum shifts toward higher wavelengths at pH=10 compared to initial conditions (pH=5.44). The time effect makes the pH decrease reasonably fast, resulting in the range returning toward the initial spectrum while the absorbance decreases. After 24h, no further changes were observed, and the pH of the solution gradually dropped to pH=7.87. The DOX spectrum at pH = 10.0 is characterized not only by a significant shift and decrease in absorbance but also by the appearance of three characteristic spectral maxima due to the presence of different tautomeric conformers in solution. In this case, we observe the same peak position while the spectrum gradually returns to its initial position after 24h. The disappearance of the three characteristic peaks is associated with the successful return of deprotonated forms to the initial state due to decreased pH. The molecule's tendency to adopt different states in an aqueous solution at pH 7.5 – 10.0 causes the self-aggregation process of doxorubicin. Both the hydrophilic sugar part of daunosamine and the hydrophobic part of anthracycline promote aggregation of the DOX molecules in different environments, similar to other amphiphilic molecules [5,30]. DLS measurements confirmed the tendency for aggregation for DOX aqueous solution with a concentration of c = 0.5 mg/mL (Table SM1).

In addition, circular dichroism (CD) was used to determine the structure of DOX molecules in aqueous solution at high concentrations (Figure 1a). CD spectra are characterized by the presence of two maxima at λ_{max1} = 350 nm and λ_{max2} = 455 nm and three minimum peaks at λ_{min1} = 295 nm, λ_{min2} = 542 nm and λ_{min3} = 550 nm. The presence of two characteristic minima at λ_{min2} = 542 nm and λ_{min3} = 550 nm confirms DOX oligomerization in the given concentration range, which correlates well with DLS results. This is supported by the results of Fülöp et al., which show that DOX aggregation occurs in aqueous solution above c = 0.5 mg/mL [30]. Fluorescence spectroscopy can be a valuable method for determining the potential DOX aggregation process. Doxorubicin exhibits fluorescence properties with a quantum yield of 4.5% in an aqueous solution [32]. It is worth mentioning that the drug in the monomeric form shows fluorescence properties with characteristic peaks with emission around λ_{em} = 560, 594, and 638 nm ($\varphi_{monomer}$=3.9×10^{-2}). At the same time dimerization occurs, the fluorescence yield decreases significantly ($\varphi_{dimmer} \approx 10^{-5}$) [33,34]. The fluorescence spectrum of DOX shows three distinct peaks at around λ_{max1} = 550, λ_{max2} = 596, and λ_{max3} = 640 nm (Figure 1b). The vibrational structures observed in the absorption and fluorescence spectra are due to symmetric modes associated with the dihydroxyanthraquinone molecule's C=O bending, backbone stretching, and -OH bending motions [33]. The spectra's shape and maximum position confirm the presence of the monomeric form of DOX at low concentrations. The trend of fluorescence intensity changes with pH shows that the protonated form of DOX exhibits the highest fluorescence, while above pH 7.5, it is successively quenched.
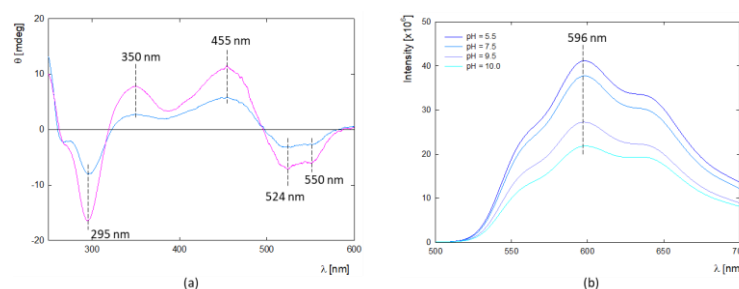

Figure 1. (a) CD spectra of aggregated forms of doxorubicin in water solution and its dependence on concentration (blue line – c = 0.5 mg/mL, pink line – c = 1.0 mg/mL). (b) Fluorescence spectra of doxorubicin and its dependence on pH (c = 2 μg/mL, H$_2$O).

Measurement of the electrophoretic mobility of doxorubicin molecules made it possible to determine their zeta potential, as illustrated in Figure 2. The analysis showed that the isoelectric point (iep), at which the molecules have a neutral charge (ζ=0 mV) occurs at pH=10.0. Below this value, the zeta potential of doxorubicin molecules is positive, which averages ζ = 35.8 ± 3.8 mV, while above this, at strongly alkaline pH, doxorubicin molecules become negatively charged. This correlates well with the results of Ryzkhina et al., who also observed a cationic form with a charge of ζ = 17.0 mV for an aqueous solution of DOX [31].
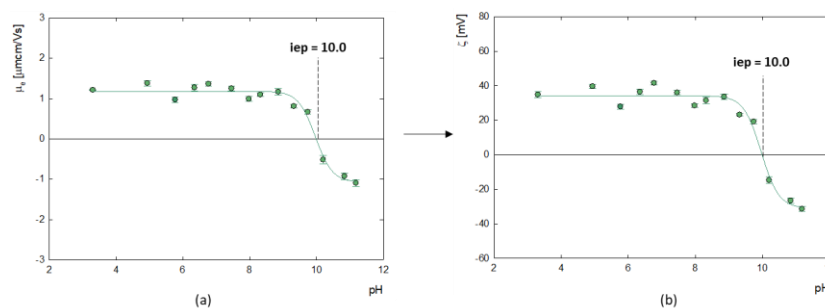

Figure 2. (a) Change in electrophoretic mobility (μ_e) and (b) zeta potential (ζ) of aqueous solution of aggregated forms of doxorubicin as a function of pH with determined value of isoelectric point (iep) (c_{DOX}= 0.5 mg/mL).

2.2. Physicochemical Properties of G4.0-DOX Complexes

2.2.1. QCM-D and MP-SPR Studies

The QCM-D method was used to determine the binding efficiency of doxorubicin to the G4.0 PAMAM dendrimer surface under physiological pH conditions (pH=7.5) and alkaline conditions (pH=8.5 – 10.0) (Figure 3b). For this purpose, a stable dendrimer monolayer was formed on the gold surface at pH 10.0, with the highest adsorption efficiency [35,36]. At each measurement, a steady and repetitive dendrimer monolayer with a thickness of d = 4.5 nm was formed, making it possible to compare the efficiency of DOX adsorption as a function of pH and concentration (Figure 3a). Layers where the G4.0 PAMAM/DOX molar ratio was 1:3 and 1:6 at pH 9.0 and 1:6 at pH 7.5 and 8.5 were characterized by dissipation < 1.0×10^{-6}. Higher dissipation values and a lack of overtone overlap were observed for the other bilayers at alkaline pH and higher DOX concentrations (Figure SM3). The G4.0 PAMAM/DOX bilayers exhibit a rigid structure for low concentrations and pH values. In contrast, the layers have viscoelastic properties for higher molar ratios and stronger alkaline pH. The properties of doxorubicin determine the nature of the formed bilayer. Under physiological pH, no adsorption of the drug on the G4.0 PAMAM surface is observed; there is a slight wash-off and loss of layer mass by about 20 ng/cm². A strong effect of pH on the adsorption efficiency of doxorubicin on the G4.0 PAMAM surface is observed, which increases with increasing pH. The gradual increase in DOX adsorbed mass begins at a slightly alkaline pH (pH = 8.5). This is related to the change in the protonation of the DOX molecule. Tautomeric forms of doxorubicin that occur at alkaline pH have a negative charge, which can promote electrostatic binding to the dendrimer's surface groups [37]. The most significant adsorption is observed when the dendrimer is electrostatically neutral (pH 10.0). Based on literature data, hydrolysis of DOX and a strong tendency to dimerization is observed in this condition [37]. The strong deprotonation of drug molecules may determine the binding efficiency of protonated dendrimer groups. On the other hand, deprotonation and subsequent formation of DOX dimers can lead to association with the dendrimer surface while forming aggregates, resulting in a strong increase in mass with increasing pH. Considering this effect, the influence of DOX concentration on adsorption efficiency under alkaline conditions (pH 9.0 – 10.0) was tested. Prepared drug concentrations corresponded to G4.0/DOX molar ratios of 1:3, 1:6, and 1:9. As shown by the results in Figure 3c, a strong effect was observed not only of increasing the pH of the drug on the adsorption efficiency but also of increasing its concentration. Thus, the highest layer was obtained for conditions when the pH of DOX was 10.0, and the molar ratio was 1:9. Adsorption of analogous bilayers using MP-SPR made it possible to determine the degree of hydration of the structure. The observed trend of mass increase as a function of pH is analogous for both methods. In the case of QCM-D, the sensor's surface excess is much higher than MP-SPR (Figure 3d). This difference is due to the presence of water, which is detected in the QCM-D method. To determine the amount of water in the adsorbed layers, the degree of hydration of the layers of three selected solutions was defined as a function of pH (pH= 9.0, 9.5 and 10.0, molar ratio of G4.0/DOX = 1:6). The use of complementary QCM-D and MP-SPR methods made it possible to demonstrate the contribution of water to the mass of the formed layers. The G4.0 PAMAM monolayer has a hydration level of 58% at pH 10.0 to 63% at pH 9.0 (Figure 3e). The relatively low degree of hydration of G4.0 PAMAM is due to the low level of protonation of the internal and external groups of the dendrimer at high pH values. How it was presented for the G6.0 PAMAM hydration degree is strongly connected with pH (83% for pH = 9.0 and dropped to 64% at pH = 10.0) [38]. A successive increase in the amount of DOX adsorbed on the surface of the dendrimer leads to an increase in water content and results in a change in the hydration of the layer up to 82%. The number of DOX per carrier molecule (N_{DOX}/1 G4.0 particle) resulting from the SPR mass of the layers was calculated. The results showed the incorporation of about 1 to 17 DOX particles per one G4.0 PAMAM particle, depending on pH. The highest efficiency complex formation was obtained for pH = 10.0 (Table 2). Results for both methods confirm the binding of DOX to the dendrimer structure under alkaline conditions. Successful functionalization of the gold sensor with a PAMAM dendrimer indicates its potential as a biosensor for quantifying bioactive molecules in biomedical applications.

Table 2. The number of dendrimer particles ($N_{G4.0}$) adsorbed on the Au sensor and doxorubicin (N_{DOX}) on the dendrimer surface in the MP-SPR method depending on the pH of DOX ($pH_{G4.0}$ = 10.0, $c_{G4.0}$ = 0.25 mg/mL, c_{DOX} = 0.06 mg/mL, H_2O).

pH_{DOX}	$N_{G4.0}$ ($\times10^{13}$)	N_{DOX} ($\times10^{13}$)	N_{DOX}/1 G4.0 particle
9.0	8.1	6.2	0.8
9.5	8.7	24.9	2.9
10.0	9.2	156.0	16.9

2.2.2. Fourier Transform Infrared (FTIR) Measurement

The formation of stable complexes of dendrimer with doxorubicin is confirmed by FTIR spectra (Figure SM5). The dendrimer spectrum (blue line) shows two main peaks at 1652 cm^{-1} and 1560 cm^{-1}, which were assigned to an amide linkage. The peak at 3284 cm^{-1} was allocated to primary amines present on the surface of the PAMAM structure [39,40]. The DOX spectrum (dark blue line) is characterized by the following peaks: 991 cm^{-1} and 1023 cm^{-1}, which are given to the skeletal ring. The following four peaks at 1083 cm^{-1}, 1117 cm^{-1}, 1214 cm^{-1}, and 1288 cm^{-1} correspond to C-N, C-O-C, and C-O stretching vibrations. Subsequent peaks at 1414 cm^{-1} and 1443 cm^{-1} were assigned to methyl and hydroxyl group bending vibration, respectively. The peak at 1580 presents N-H bending and C-N stretching vibrations[41]. FTIR spectra of G4.0-DOX complexes confirm the interactions between the components. Despite maintaining a constant dendrimer concentration in the complexes, signals at 1562 cm^{-1} and 3289 cm^{-1} are enhanced. A shift of the signal at 1562 cm^{-1} to 1577 cm^{-1}, originating from internal amide groups, is observed. The peak from the surface amine groups at 3289 cm^{-1} thickens and shifts to 3284 cm^{-1}, confirming interactions with the drug molecule. In addition, the complexes show a drug-specific peak at about 3500 cm^{-1}, attributed to water molecules bound to drug molecules [41].

2.2.3. Binding Constants and Thermodynamic Parameters of G4.0-DOX

The fluorescence properties of DOX can help study carrier-drug interactions and imaging in biological systems [42,43]. In the present study, fluorescent properties of doxorubicin were used to determine G4.0-DOX binding constants (K_a) by fluorescence quenching through the presence of a dendrimer (Figure 4). A summary of the obtained binding constants is given in Table 3. The values of binding constants equal $K_{7.5}$=2.07×10^6, $K_{9.0}$=9.38×10^2, $K_{9.5}$=7.01×10^2 and their values decrease with increasing pH. The determined values of binding constants at alkaline conditions are $K_{9.0}$=9.38×10^2 M^{-1} and $K_{9.5}$=7.01×10^2 M^{-1} and they are close to the values that we obtained in previous work using UV-vis with Hill's method ($K_{9.0}$=2.39×10^2 and $K_{9.5}$=2.73×10^2) [29]. The value of the binding constant at pH 7.5 is close to that obtained by Chanphai et al. for the same system in PBS buffer at physiological pH as well (K=1.6×10^6) [44]. In contrast, the G4.0-DOX system at physiological pH was the only one among the studied systems for which thermodynamic parameters could be determined using calorimetric studies. The ITC measurements were performed for the G4.0-DOX system in PBS buffer at pH = 7.4. Measures at alkaline pH in water were impossible due to the high concentration of DOX in the syringe and the associated strong aggregation. Calorimetric measurements indicate that the G4.0 PAMAM binds DOX in the endothermic process ($\Delta H > 0$) with a significant positive entropy change. All thermodynamic parameters obtained for the G4.0PAMAM/DOX system are collected in Table 3. An independent model is used when the multiple binding sites on a macromolecule are present and are independent. Referring to the shape of the obtained isotherm, it can be assumed that the binding sites are not identical (Figure SM6). The best fit for the results obtained is a multiple site model that may be related to non-identical binding sites or interactions [45]. Binding sites have different affinity; while all binding sites are similar, it could be a cooperative process. The first binding site (K_{a1} = 1.215 × 10^5 M^{-1}; K_{d1} =8.232 × 10^{-6} M) had a stronger association than the second one (K_{a2} = 1.065 × 10^2 M^{-1}; K_{d2} = K_{d1} =9.390 × 10^{-3} M). The enthalpy of site 1 is ΔH_1 = 9.068 kJ/mol, and the poorer binding at site 2 was entirely attributed to a less favorable enthalpy

(ΔH_2= 198.9 kJ/mol). Considering all the parameters, the change in enthalpy, the difference in entropy, and the change in Gibbs free energy, it can be seen that in the system under study, the reaction occurs spontaneously with the preferred contribution of the entropic factor. The enthalpy change is much lower than the -TΔS value, which indicates a spontaneous process of binding DOX to G4.0 PAMAM at the studied temperature [46]. The binding enthalpies for considered two binding sites are positive, and their values equal ΔH_1 = 9.068 and ΔH_2 = 198.9 kJ/mol, respectively. The binding entropies are also positive with values ΔS_1 = 1.278×10^2 J/mol·K and ΔS_2 = 7.058×10^2 J/mol·K. Rise entropy value indicates that the system becomes more disordered. The most preferred effect of the G4.0-DOX interaction is the effect of desolvation (hydrophobic force) and conformational changes [47]. This is most likely due to the release of dissolution molecules surrounding the DOX molecules and filling the binding sites of the G4.0 PAMAM dendrimer.
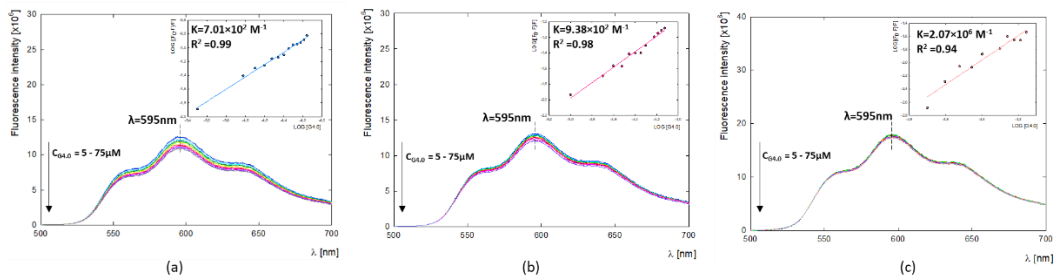

Figure 4. Fluorescence emission spectra of G4.0 PAMAM-DOX systems presented for: (a) G4.0-DOX at pH 7.5; (b) G4.0-DOX at pH 9.0; (c) G4.0-DOX at pH 9.5 and LOG((F0-F)/F) versus LOG [G4.0] plots.

Table 3. Thermodynamic parameters obtained for G4.0/DOX system in ITC experiments. Data for the titration of 2.12 mM DOX into 0.0176 mM G4.0 in PBS buffer, pH 7.4. T= 25°C.

Binding site	K_a (M^{-1})	n	ΔH (kJ/mol)	K_d (M)	ΔS (J/mol ·K)	ΔG (J/mol)
1	$1.215 \times 10^5 \pm 0.55$	6.18 ± 0.30	9.068 ± 0.26	8.232×10^{-6}	1.278×10^2	-2.902×10^4
2	$1.065 \times 10^2 \pm 0.51$	17.05 ± 4.85	198.9 ± 57	9.390×10^{-3}	7.058×10^2	-1.143×10^4

2.2.4. Electrophoretic Mobility

The values of zeta potential as a function of pH for the dendrimer and the G4.0 PAMAM-DOX complex were calculated from electrophoretic mobility (μ_e) measurements and presented in Figure 5. Results show changes in the zeta potential of G4.0 PAMAM as a function of pH, ionic strength and solvent (Figure 5a). The presence of amine functional groups on the surface of the dendrimer determines the charge changes. In the aqueous solution, G4.0 PAMAM has a high zeta potential (69.7mV for pH=7.5), which successively decreases with increasing pH and reaches the isoelectric point (iep) at pH=9.9. Increasing the ionic strength causes the zeta potential to drop to 37.7 mV for 0.15M NaCl and 13.9 mV for 0.15M PBS (pH=7.5), consistent with other literature data [48]. Depending on the solvent, the isoelectric point is shifted to pH_{iep}=10.3 and pH_{iep}=9.0 for NaCl and PBS, respectively. The zeta potential of the complex (Figure 5b) was measured immediately after complex formation and after the dialysis process. Dialysis was used to remove DOX molecules that were not bound to the carrier. Slight changes in the zeta potential value generally characterize the course of the curves before and after dialysis. In the pH range 4-6, an increase in the value of the zeta potential after dialysis is observed concerning the initial zeta potential of the complex. In this pH range, DOX exists in a protonated form, thus being released from the complex due to electrostatic repulsion. These measurements confirm the immobilization of DOX molecules on the surface of the dendrimer structure in a reversible manner.
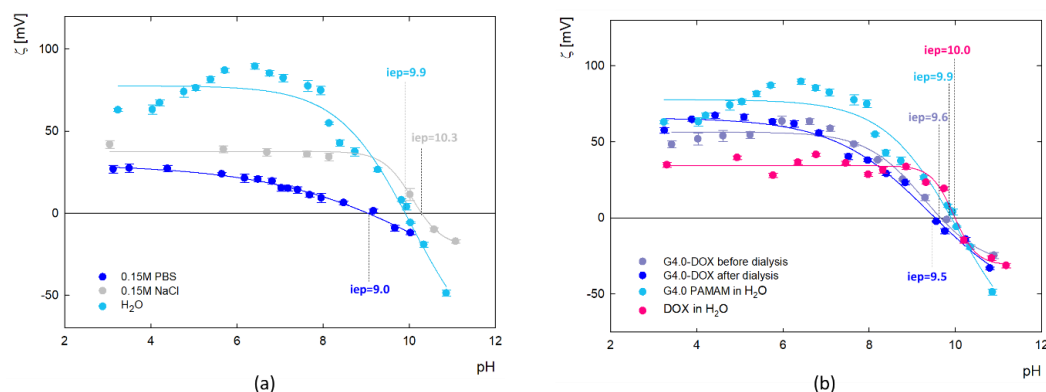
Figure 5. Change in the zeta potential (ζ) of G4.0 PAMAM dendrimer depending on ionic strength and solvent (a) and complexes with doxorubicin before and after dialysis (b) with determined values of isoelectric point (iep) (H_2O, molar ratio 1:6, pH 9.5).

2.3. Cytotoxicity and Release Studies

2.3.1. In Vitro MTT Assay

Doxorubicin is a commonly used chemotherapeutic agent, and it was used as a model drug for validating nanosystems to deliver drugs depending on the type of cell [13]. Nanosystems based on dendrimers improved targeting, controlled release, enhanced bioavailability, and reduced organ toxicity, making them promising candidates for cancer treatment [49]. Zhang et al. also conjugated PAMAM dendrimers with doxorubicin, modified these nanocarriers by folic acid (FA), and showed anticancer effects against epidermoid carcinoma (KB cells) [50]. Marcinkowska et al. used PAMAM dendrimers conjugated with doxorubicin and monoclonal antibody (trastuzumab) versus breast cancer cells. The authors demonstrated that PAMAM–dox–trastuzumab conjugate was more effective for tumors with HER-2 overexpression – here SKBR-3 cells [51]. In the present study *in vitro* tests for dendrimers and their complexes with doxorubicin were conducted against immortalized keratinocytes (HaCaT) as a model of normal cell line and six cancer cell lines (A375, HT-29, NCL-H23, LoVoDX, MCF-7 and MCF-7/DX). According to our previous experience, we have selected 24 and 72 hours, commonly chosen endpoints for cytotoxicity assays and allow researchers to capture variations in cellular response over time. More extended incubation periods, such as 72 hours, provide insights into whether cytotoxic effects persist, diminish, or escalate over time. This information is crucial for evaluating substances' safety profile, especially those intended for prolonged exposure, such as pharmaceuticals or environmental pollutants. Cytotoxicity tests showed no cytotoxicity of G4.0 PAMAM-empty dendrimers against normal and cancer cells (Figure 6). A selective anticancer activity of the G4.0 PAMAM-DOX-1 complex was observed against A375 human skin cancer cells and NCL-H23 human lung cancer cells, as demonstrated in Figure 6.

No significant cytotoxic effect was observed in the case of drug-resistant cells MCF-7/DX and LoVoDX (Figure SM7). In the case of both breast cancer cell lines (sensitive and resistant), G4.0 PAMAM-DOX-3 for 8 μM induced a significant viability decrease below 40%. In turn, keratinocytes were more sensitive to G4.0 PAMAM-DOX-1 after 24h exposure, and after 72h, all nanocarriers induced similar cytotoxic efficacy. The results confirmed the effectiveness of dendrimers and G4.0 PAMAM-DOX complexes firmly on cell type. In some cases, the therapeutic effect of DOX can be enhanced by the presence of G4.0 PAMAM dendrimers. To extend the analysis of anticancer activity, IC50 dose for free DOX and G4.0-DOX complexes was determined (Table 4). Calculation of IC50 compound was possible only for cell lines for which significant cytotoxicity was observed, i.e. normal keratinocytes (HaCaT), malignant melanoma (A375) and lung cancer (NCl-H23). After 24h incubation of keratinocytes with free DOX, the IC50 value was 1.57 μg/mL (2.61 μM). A similar value after 24h of incubation with the same line was recorded by Pessila et al. (IC50 = 2.72 μM) [52]. After 72h of incubation, doxorubicin's IC_50 drastically decreased about 4 times and was 0.37 ug/mL (0.58

µM). To determine if any of the tested compounds are more selective towards cancer cell lines than normal keratinocytes, the selectivity index (SI) was calculated based on the obtained IC_{50} values. SI is a pure IC_{50} value ratio in a non-cancer cell line (HaCaT) to IC50 value in a cancer cell line (A375 and NCl-H23). Study demonstrates poor selectivity of free DOX towards malignant melanoma (SI=0.29) and lung cancer cells (SI=0.61). An improvement in selectivity was noted when DOX was complexed with G4.0 PAMAM at a molar ratio of 1:12 and pH = 9.5, where its selectivity was increased by 147 % (SI = 0.79) and 21% (SI = 0.81) against malignant melanoma and lung cancer, respectively.
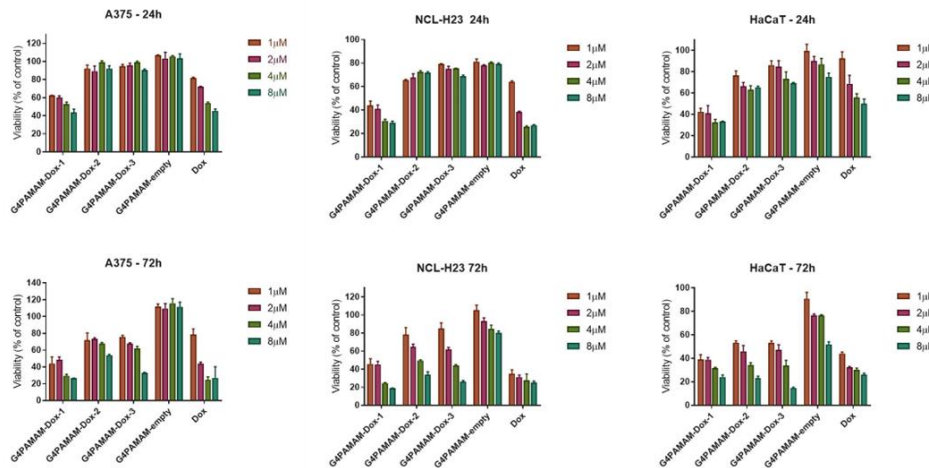

Figure 6. The cytotoxic effect of G4.0 PAMAM nanocarriers against human cancer (A375, NCL-H23) and immortalized cells (HaCaT) as a model of normal cell line, evaluated by MTT assay after 24 and 72h. # p≤0.05.

Table 4. The half maximal inhibitory concentration (IC50) values and the selectivity index (SI) values of doxorubicin alone (DOX) compared to G4.0-DOX complexes in 3 cell lines: normal keratinocytes (HaCaT) malignant melanoma (A375) and lung cancer (NCl-H23) following a 72 hours incubation with the compounds.

Cell line	HaCaT		A375		NCl-H23	
Compound IC50						
	IC50 [µg/mL]	IC50 [µM]	IC50 [µg/mL]	IC50 [µM]	IC50 [µg/mL]	IC50 [µM]
DOX	0.37	0.64	1.14	2.41	0.55	0.95
G4.0-DOX 1:6	0.64	1.10	4.22	7.28	3.64	6.28
G4.0-DOX 1:12	0.58	1.00	0.73	1.26	0.72	1.24
G4.0-DOX 1:24	0.81	1.40	-	-	2.28	3.93
G4.0-DOX 1:50	0.82	1.41	3.57	6.16	1.89	3.26
Compound SI						
DOX	-		0.32		0.67	
G4.0-DOX 1:6	-		0.15		0.18	
G4.0-DOX 1:12	-		0.79		0.81	
G4.0-DOX 1:24	-		-		0.38	

G4.0-DOX 1:50	-	0.23	0.43

2.3.2. G4.0 PAMAM Internalization In Vitro

The imaging presented in Figure 7 represents the intracellular distribution of free or encapsulated doxorubicin in A375 and HaCaT cells. Figure 7a shows distributions of nanosystems in living cells post 24h after exposure with a clear difference between the free DOX and DOX loaded in nanosystems. Free doxorubicin is localized in nuclei and incorporated in G4.0 PAMAM systems, and it is distributed in the whole cytoplasm of both treated cell lines. The colocalization imaging of fixed cells with nanosystems and stained nuclei confirmed the distribution of doxorubicin in cancer cells and partially in normal cells. In turn, G4.0 PAMAM-DOX is distributed in the cytoplasm and nuclei. However, in the case of normal cells, after 24h we could also observe nuclear DOX distribution, and post 72h DOX in nanosystems was translocated to the cytoplasm (Figure 7b). To better understand the behavior mechanism of the G4.0-DOX at the cellular level, the profile of DOX release from complex was determined (Figure 8a). Maintains DNA tension occurs. The other involves intercalation of DOX into the DNA strand, preferably at the cyto-sine-guanine nucleotide pair. The present mechanisms explain the accumulation of free DOX in cell nuclei [53].
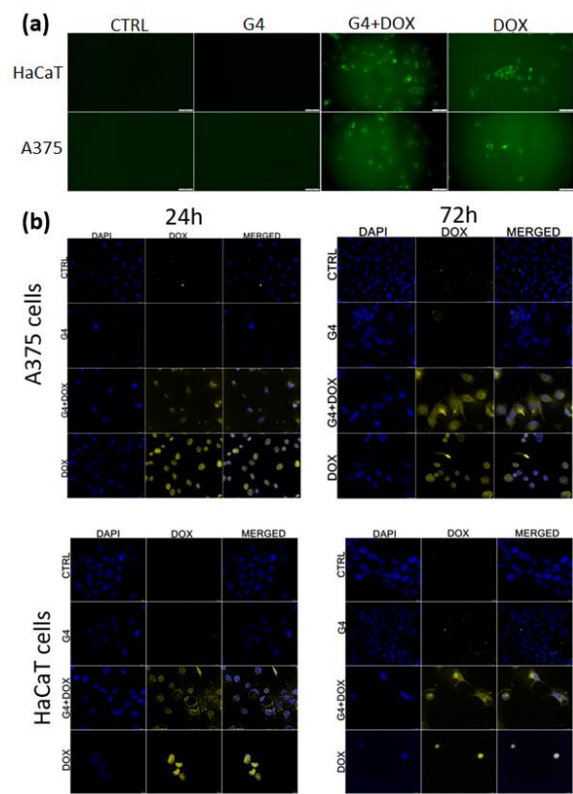

Figure 7. Internalization of G4.0 PAMAM-DOX, and free DOX by confocal microscopy in A375 and HaCaT cells: intravital analysis after 24h (a) and analysis of fixed cells after 24 and 72h (b). DOX- green color; nuclei- DAPI blue color.
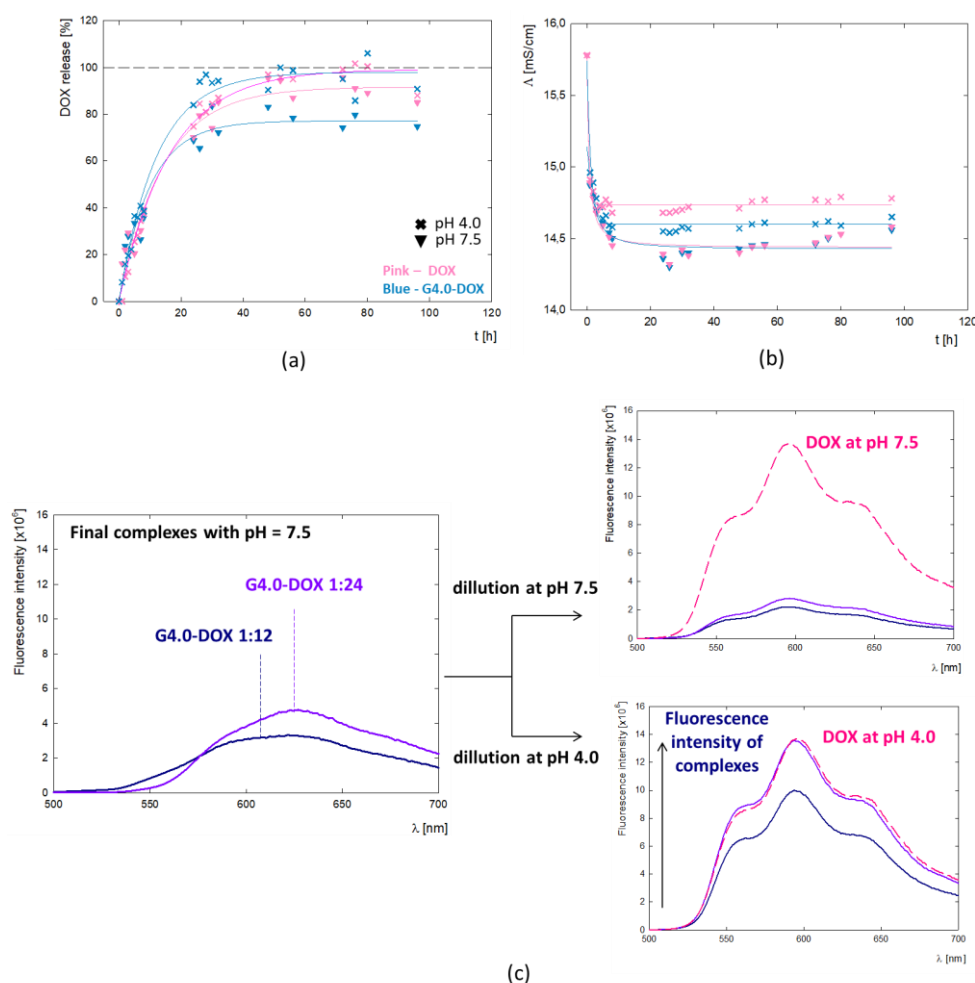
Figure 8. (a) Release profile of doxorubicin from complex compared to DOX of the same concentration (c=38 μM) into PBS buffer at pH 7.4. Triangle - final complex at pH 7.5; cross - final complex after reducing to pH=4.0. (b) Change in electrolytic conductivity of PBS buffer during release assay. (c) Fluorescence spectra of G4.0-DOX complexes at molar ratios of 1:12 and 1:24, their changes after dilution in water at pH 7.5 and pH 4.0 and comparison with reference DOX solution at the same pH and concentration (c=5 μM).

To better understand the behavior mechanism of the G4.0-DOX at the cellular level, the profile of DOX release from the complex was determined (Figure 8a). The tests were conducted in two variants - for the final G4.0/DOX complex at pH 7.5 and after reducing its pH to 4.0. In the presented DOX release profile, two main process steps are observed: a rapid release of the active substance during the first 24h of incubation and a slow process for the next 72h. This may be related to the location of the molecules in the dendrimer structure and thus to a change in interactions and, consequently, the method of drug release from the carrier. It is expected that molecules located on the surface of the carrier can be released into the environment with-out a barrier. In the case of molecules contained inside the structure, their release may be difficult due to steric interactions resulting from the level of protonation of functional groups present in the carrier itself. This confirms the gradual release of DOX from the complex. After 24 hours, 60% of the drug is released, while 70% is released after 72 hours. The two-step mechanism of drug release from the polymer structure has a positive therapeutic effect as it prolongs the drug release. The drug bound to the dendrimer remains in the cytoplasm, where it also plays its cytotoxic role. The DOX release rate up to 96 hours is identical regardless of pH.

Based on the doxorubicin release curves, the kinetic parameters of the process were determined (Table 5). The value of the rate constant for the release of DOX from the complex (k_1) is similar regardless of pH. The amount of DOX released per hour equals 8.2% and 9.1% at pH =4.0 and pH = 7.5, respectively. A significant difference is observed at the final stage of the process, where the maximum percentage of released drug is A_{max}= 73.3% and A_{max}= 97.9% of the active substance is released from the complex at pH = 7.5 and pH = 4.0, respectively. This apparent difference may be due to the overall dissociation of DOX from the complex due to the change in ionization form at pH=4.0. Fluorescence spectroscopy revealed fluorescence quenching of the drug upon binding to G4.0 PAMAM. At pH = 7.5, despite the strong fluorescence of the reference system being the DOX solution, no signal from the drug is observed in the spectrum of the complexes. When the pH of the G4.0PAMAM-DOX system is lowered to pH = 4.0, a peak appears in the spectrum with emission at λ_{em} = 596nm, characteristic of the fluorescence emission from doxorubicin (Figure 8c). At pH 4.0, the doxorubicin enclosed inside the complex is released. The mechanism of drug release from the carrier structure in an acidic environment is also confirmed by release tests.

Table 5. Maximum percentage of released mass (A_{max}) and release rate constant (k_1) of DOX from the complex compared to free drug into PBS buffer at pH=7.4.

	pH	A_{max} [%]	k_1 [h^{-1}]	R^2
DOX	4.0	99.2 ± 1.7	0.062 ± 0.003	0.99
	7.5	91.6 ± 2.6	0.070 ± 0.008	0.97
G4.0-DOX	4.0	97.9 ± 2.1	0.082 ± 0.007	0.98
	7.5	73.3 ± 2.4	0.091 ± 0.012	0.95

3. Discussion

Doxorubicin can take different tautomeric forms – protonated and deprotonated depending on the pH of the solution. Under physiological conditions, the predominant form is protonated with a positive charge on the amino group [54]. Its presence is directly related to the mechanism of action and DOX-DNA interaction, which is stabilized, i.e., by electrostatic interactions between the cationic amino sugar of doxorubicin and the anionic phosphate backbone of DNA [55]. Stability studies of doxorubicin as a function of pH and time conducted using UV-vis spectroscopy showed that depending on the conditions, a part of the drug concentration is degraded. The spectrum of the drug at pH=10.0 differs significantly from the others, where three characteristic maxima are observed. Florencio et al., using theoretical methods, investigated the effect of four DOX tautomers and their deprotonated forms as a function of pH on doxorubicin's spectral profile. They showed that the spectrum of DOX under alkaline conditions (pH =10.08) is characterized by three peaks around 500, 550, and 600nm, corresponding to the simultaneous contribution of the four deprotonated conformers [56]. Doxorubicin's tendency to self-aggregation under physiological conditions may be responsible for its cytotoxicity, cellular immunity, or reduced anticancer activity. The tendency for the drug to self-aggregate was confirmed for concentration > 0.5mg/mL, and the process was shown to intensify at pH > 9.0, which is related to the presence of various DOX conformers with opposite charges in the aqueous solution. Fülöp et al. pointed out the effect of DOX concentration on self-aggregation in aqueous solution using the permeation technique and showed that dimers and trimmers were observed at deficient concentrations of doxorubicin. At a concentration of 0.5 mg/mL (8.6×10^{-3} M), aggregates containing about 40 molecules were present [30]. In contrast, using circular dichroism (CD) spectra, Anand et al. demonstrated the presence of DOX dimers in phosphate buffer at pH 7.4 at a concentration $\geq 1.0 \times 10^{-5}$ M [57], while Maruf et al. report a limit of 6.9×10^{-5} M, above which DOX begins to aggregate in PBS buffer at pH 7.4 [3]. In the present study, the effect of pH changes on the spectrum of doxorubicin at low concentrations (2 μg/mL) was performed using fluorescence spectroscopy. The spectra's shape and maximum position (λ_{em}=596 nm) confirm the presence of the monomeric form of DOX at low concentrations [34]. As has already been demonstrated in the literature, the DOX dimerization or polymerization can strongly disrupt its fluorescence, leading to a significant reduction in intensity and a bathochromic shift in the spectrum

[33,34]. In our case, a change in the spectrum is not observed, proving the absence of DOX polymers at the studied concentration and pH. The significant reduction in intensity with increasing pH may be due to partial degradation of the drug and the subsequent extinction of its fluorescence.

The critical issue that was studied in the present work is the effect of the drug molecule's charge and form on interactions with the dendrimer carrier. Our previous work demonstrated that G4.0 PAMAM can efficiently bind DOX in an alkaline environment (pH > 9.0) with a loading capacity of LC = 4.80 – 40.16 %, depending on conditions [29]. Liping et al. determined the efficiency for the same system in the aqueous environment at LC = 8.1 – 8.8% [17]. Also, many other works are focused on developing an effective DOX delivery system based on dendrimer nanocarriers [58,59]. Changes in the electrophoretic mobility values of the formed complex and FTIR spectroscopy monitored the successive immobilization of DOX to the G4.0 PAMAM structure. Using the QCM-D method, the influence of pH on the efficiency of the formation of the G4.0 PAMAM-DOX complex in dynamic conditions was tested. Effective adsorption of DOX to the dendrimer layer was observed for pH > 8.5, and the highest for pH = 10.0. Both pH and drug concentration have a significant impact on the viscoelastic properties of the formed G4.0/DOX bilayer. At pH < 9.0 and in the range of low drug concentrations (molar ratio G4.0/DOX 1:3), the bilayers formed are stiff. Bilayers formed at higher DOX concentrations and pH ≥ 9.0 show an increase in viscoelastic properties. Based on QCM-D and MP-SPR measurements, the degree of hydration of both the G4.0 PAMAM monolayer (58-63% at pH 9.0-10.0) and the G4.0/DOX bilayers (72-82% at pH 9.0-10.0) was determined. The presence of drug molecules causes a significant increase in the system's hydration. The affinity of the drug to the dendrimer was determined under basic conditions using fluorescence spectroscopy ($K_{7.5}$ = 2.07 × 10^6, $K_{9.0}$ = 9.38 × 10^2, $K_{9.5}$ = 7.01 × 10^2). The course of the ITC isotherm indicates that two different types of active sites, differing in affinity, are involved in forming the complex with doxorubicin (K_{a1} = 1.215 × 10^5 M^{-1}, K_{a2} = 1.065 × 10^2 M^{-1}). The ΔG value indicates that we are dealing with an endothermic process. Since the ΔS and ΔH parameters have positive values, the hydrophobic interaction has a significant contribution to the formation of the complex. Under basic conditions, the dominant form of doxorubicin is the tautomeric form with a negative charge, which, through electrostatic interaction, is immobilized on the surface of the carrier, which under these conditions has a positive charge. It should be noted that other tautomeric forms also occur under these conditions and may prefer to be located in the hydrophobic interior of the polymer.

In vitro studies have shown specific anticancer activity of G4.0-DOX complexes and increased selectivity towards malignant melanoma and lung cancer cell lines. Doxorubicin contained in the complex is less toxic than free DOX towards the HaCaT cell line. A significant decrease in HaCaT cell viability is due to the fact that they exhibit high levels of topoisomerase I activity, which is significantly inhibited by doxorubicin [52]. Complexation of doxorubicin with a dendrimer carrier decreased its IC$_{50}$ against HaCaT cells by up to more than 2 times indicating protection from the drug's harmful effects on normal cells. In addition, a destructive impact of free DOX on the HaCaT cell membrane is observed, while binding to the carrier significantly reduces this effect, proving less harmful interference of the complex against keratinocytes. The dendrimer-bound drug localizes to the nucleus and the cytoplasm, while the free drug accumulates preferentially in the cell nucleus. The diversified distribution within the cell indicates a specific interaction of both forms at the molecular level, with no disruption of the therapeutic effect of the drug administered in the form of a complex. It should be emphasized that due to the structure of the dendrimer, doxorubicin molecules are released from the complex in two ways. Particles that are electrostatically immobilized on the surface of the carrier structure are easily released, while the molecules that are bound inside by hydrophobic interactions and are more difficult to release. Based on the release curves, it was determined that at pH=7.4 73% of the drug was released, while at pH=4.0 up to 100%. The release of more significant amount of doxorubicin at acidic pH comes directly from the change in the protonation of the carrier, the opening of the polymer structures, and thus the availability of drug molecules located in hydrophobic pockets. These findings support the pH-regulated mechanism of doxorubicin release from the G4.0-DOX complex. The other available studies also indicate that minimum micromolar DOX concentrations were active in cancer cells, e.g., loaded in polypeptide nanocarriers in lymphoma

[60]; when combined with L-Canavaine against HeLa, Caco-2, MIA PaCa-2, BxPC-3, HEP G2, SK-HEP-1 [61]; DOX in G4PEG against MCF-7 cells revealed significantly higher concentration 1.3mM [62]. The PAMAM dendrimers in our study are highly branched, nanoscale polymers that can form complexes with DOX at various binding ratios. These ratios represent different levels of drug loading, which can influence the overall physicochemical properties of the complexes, including their size, charge, and drug release profile. Several factors could explain the observed trend of increasing IC$_{50}$ values with higher DOX loading ratios: (1) drug release dynamics - At higher binding ratios (e.g., 1:6 and 1:12), the interaction between DOX and the dendrimer may result in a more stable complex, which could slow down the release of DOX. This slower release rate may lead to reduced immediate cytotoxicity, as reflected in higher IC50 values; (2) dendrimer saturation - As the binding ratio increases, the dendrimer surface may become saturated with DOX molecules. This saturation can lead to changes in the complex's overall conformation and reduce the availability of free DOX to interact with cellular targets; (3) Steric hindrance and accessibility - higher DOX loading may cause steric hindrance, affecting the ability of the DOX molecules to access and penetrate the cancer cells effectively. This reduced accessibility can result in lower cytotoxicity; (4) aggregation and stability - At higher binding ratios, there is a potential for forming larger aggregates, which could alter the cellular uptake and distribution of the complexes. These aggregates might be less efficient in delivering DOX to the intracellular targets, leading to decreased cytotoxic effects.

4. Materials and Methods

4.1. Materials

Poly(amidoamine) dendrimers generation 4.0 (G4.0 PAMAM) was acquired from Dendritech, Inc. (Michigan; Midland, MI, USA), Doxorubicin hydrochloride (DOX) from Ambeed (Arlington, Illinois, USA), deuterium oxide (D$_2$O, 99.9 atom % D) was supplied by Deutero GmbH (Kastellaun, Germany). Solutions were prepared in deionized water, and the pH was adjusted using sodium hydroxide (NaOH) and hydrochloric acid (HCl) from Chempur (Poland). G4.0 PAMAM solutions for electrophoretic mobility measurements were additionally prepared in Dulbecco's phosphate-buffered saline (PBS) and sodium chloride (NaCl) from Sigma-Aldrich (Saint Louis, Missouri, USA).

4.2. Dynamic Light Scattering (DLS)

The diffusion coefficient of the DOX in water solution was determined using a Malvern Nano ZS analyzer (Malvern, Worcestershire, UK). The self-diffusion coefficient (D) allowed to calculate the hydrodynamic radius (R$_H$) of the dendrimer using the Stokes-Einstein equation:

$$R_H = \frac{k_B T}{6\pi\eta D} \quad (1)$$

where k_B is the Boltzmann constant, T is the absolute temperature, and η is the viscosity of the solution. Doxorubicin concentration was 0.5 mg/mL. The pH of the solution was adjusted using sodium hydroxide (NaOH) with a concentration of c = 0.1 M.

4.3. Quartz Crystal Microbalance with Dissipation Monitoring (QCM-D)

The adsorption process of G4.0 PAMAM/DOX bilayers on the gold (Au) surface was carried out using the Q-Sense E1 device (Biolin Scientific, Finland). During the measurements, two parameters were monitored: the change in the resonance frequency (Δf) and the change in energy dissipation (ΔD). The first layer was formed by the G4.0 PAMAM dendrimer itself, whose aqueous solution was adsorbed each time under constant conditions (c = 17.6 µM, pH= 10.0). DOX bilayer was adsorbed in two variants. The first variant was pH-dependent, while the second variant was concentration-dependent. The pH range was 7.5 – 10.0, while the drug concentration corresponded to G4.0 PAMAM/DOX molar ratios of 1:3 – 1:9. For rigid layers, the mass adsorbed on the sensor surface (Γ_{QCM-D}) was calculated based on the Sauerbrey model for overtone n = 7 using Qtools software. The mass adsorbed on the sensor surface for viscoelastic layers was calculated based on the Voigt model using e Qsense Dfind, Biolin Scientific, Espoo, Finland software based on the measurement results for 3–11 frequency overtones.

The QCM-D technique assumes that when a substrate layer is adsorbed onto the sensor surface, the resonant frequency (f) decreases with increasing adsorbed mass (Γ_{QCM-D}) [63]. Rigid or viscoelastic properties characterize adsorbed layers and can be described by Sauerbrey or Voigt models, respectively. When adsorbed mass is uniformly distributed over the sensor surface and exhibits low energy dissipation ($0 - 1.0 \times 10^{-6}$) we can consider such a layer rigid [64]. Then, the frequency shift (Δf) is proportional to the adsorbed mass per unit area ($\Delta\Gamma_{QCM-D}$) in the Sauerbrey model [63,65]:

$$\Gamma_{QCM-D} = C_f \frac{\Delta f}{n} \quad (2)$$

where Δf — changes in the resonance frequency (Hz), C_f—constant characteristic for quartz crystals (C_f= 17.7 ng/cm^2), n—number of overtones (in the present case n=7).

The Kevin-Voigt viscoelastic models relate the measured dissipation factor (D), whose values exceed 1.0×10^{-6} [64,65]. In the Voigt model, multiple Δf and ΔD data obtained at several overtones are used to calculate the viscoelastic properties of the adsorbed layer:[63]

$$G^* = G' + iG'' = \mu_1 + i2\pi f\eta_1 \quad (3)$$

Where f is the resonant frequency, G^* is the complex shear modulus, G' is the storage modulus, and G'' is the loss modulus [63]. The mass calculation using the Voigt model was performed using Qsense Dfind software.

4.4. Multi-Parametric Surface Plasmon Resonance (MP-SPR)

G4.0 PAMAM/DOX bilayers adsorption measurements on the gold surface (Au) were performed using the MP-SPR Navi™ 200 apparatus (BioNavis Ltd., Finland), a goniometer coupled to a prism (Krechmer mode). The system has two separate channels, each of which can emit wavelengths of λ = 670 and λ = 785 nm. The MP-SPR apparatus worked in a wide angular scan range from 40 to 78°. All experiments were performed at a constant flow rate of 50 μL/min. The immobilization of the molecules on the Au sensor surface is monitored by registering intensity changes in the set angle or changes in the resonance angle's value over time. The excess of the mass of adsorbed particles determined using MP-SPR (ΓMP-SPR) on the gold surface is calculated utilizing the following equation [38,64]:

$$\Gamma_{MP-SPR} = \frac{\Delta\Theta_{SPR}k}{\frac{dn}{dc}} \quad (4)$$

where $\Delta\Theta_{SPR}$ is the change in the MP-SPR angle, k is an MP- SPR instrumental constant, and dn/dc is the refractive increment; k =1x10^{-7} nm/deg for λ = 670 nm and dn/dc $\approx$ 0.239 cm^3/g for G4.0 PAMAM dendrimer.

The hydration degree of the layers was calculated from the equation [38]:

$$\Gamma^{H_2O} = \frac{\Gamma_{QCM-D} - \Gamma_{MP-SPR}}{\Gamma_{QCM-D}} \times 100 \ [\%] \quad (5)$$

Where Γ_{MP-SPR} is the adsorbed from MP-SPR, Γ_{QCM-D} is the adsorbed mass from QCM-D and Γ^{H_2O} is a fraction of water in adsorbed film.

4.5. Fourier-Transform Infrared Spectroscopy (FTIR)

Fourier-transform infrared spectroscopy (FTIR) measurements were performed using a Nicolet iS50, Thermo Fisher Scientific, MA/USA FTIR spectrometer with the SMART SAGA specular reflection (SR) accessory. Measurements were conducted on samples adsorbed on the gold surface layer with a thickness of 100 nm deposited on the glass plate by vapor deposition. Measurements were made for aqueous solutions of doxorubicin with the concentration of 0.24 mg/mL and G4.0-DOX complexes prepared at molar ratios of 1:6, 1:12 and 1:24 and constant dendrimer concentration (c = 0.25 mg/mL). The encapsulation efficiencies for the tested nanosystems were respectively: EE = 32.76%, EE = 35.82%, EE = 40.16%. The pH of all solutions was adjusted to pH = 9.5. For each sample, a drop of the solution was applied to a clean gold surface and allowed to evaporate under cover. FTIR spectra were recorded in the wavenumber range of λ = 700 to 4000 cm^{-1}. 512 scans were averaged for each spectrum with a spectral resolution of 4 cm^{-1}. Before each measurement, the background spectrum of the clean surface was recorded, and then it was automatically subtracted from the sample spectrum. Omnic software (Thermo Fisher Scientific, MA/USA) was used for data analysis.

4.6. Electrophoretic Mobility Measurement

Electrophoretic mobility (μ_e) was determined using a Malvern Nano ZS analyzer (Worcestershire, UK). All electrophoretic mobility measurements were conducted in the pH range of 2.0 – 11.0. The zeta potential was related to the electrophoretic mobility via Henry's equation. For the calculations, the Smoluchowski limit ($f(\kappa a)$ = 1.5) was applied for most of the solutions. Only for G4.0 PAMAM in water the Hückel limit ($f(\kappa a)$ = 1.0) was used. Pure DOX solution was measured in water with a drug concentration of c=0.5 mg/mL (c=0.86 mM). Pure G4.0 PAMAM solutions were measured depending on the solvent: NaCl (I=0.15 M) and PBS buffer (I=0.15M, pH =7.5) in deionized water. The dendrimer concentration was c=1 mg/mL (70 μM). G4.0 PAMAM–DOX complex measurements were made in water with a constant dendrimer concentration of c = 1 mg/mL (c = 70 μM). Complexes were prepared at G4.0/DOX molar ratio 1:6 and initial pH = 9.5 (EE = 32.76%,). The first measurement variant was for the complex without dialysis, while the second was for the complex after dialysis, where drug particles not bound to the dendrimer were removed. The complexes were dialyzed using Slide-A-Lyzer™ Dialysis Cassettes (MWCO 10.0 kDa), Thermo Fisher (Waltham, MA, USA). Dialysis was conducted in deionized water for 24h in darkness. The pH of solutions was adjusted using sodium hydroxide (NaOH) with a concentration of c = 0.1 M and hydrochloric acid (HCl) with a concentration of c = 0.05 M.

4.7. Circular Dichroism

Circular Dichroism (CD) measurements were performed at a spectrometer (Jasco, MD, USA) with a 10nm cuvette. CD spectra for DOX solutions were recorded in water for drug concentrations of 0.5 mg/mL (0.86 mM) and 1.0 mg/mL (1.72 mM). The spectra were recorded for two wavelength ranges of λ=240 – 450 nm and λ=250 – 650 nm with a resolution of 1 nm, while the scanning speed was equal to 50 nm/min.

4.8. Fluorescence Spectroscopy

Corrected fluorescence emission spectra of free Doxorubicin and G4.0-DOX complexes were obtained on a Fluorolog spectrofluorometer (HORIBA Jobin Yvon Ltd., Middlesex, UK) using 1 nm resolution, with both emission and excitation monochromator slits set to 5 nm. Samples in plastic cuvettes, 1x1x4 cm, with relevant solutions were prepared immediately before the measurements. Cuvettes were covered by parafilm to minimize the air exposure of the samples, which would accelerate the sample degradation and decrease the pH value. Fluorescence spectra of DOX with a concentration of c = 2 × 10^{-3} mg/mL (36 μM) in water were performed in a pH range of 5.5 – 10.0. To determine the binding constants, samples containing 0.5 mL of DOX with a concentration of c = 2.9 × 10^{-4} mg/mL (5 μM) were mixed by adding 0.5 mL of G4.0 PAMAM solution to obtain a final dendrimer concentration in the range of c = 7.1 × 10^{-3} – 0.1 mg/mL (5 – 75 μM). The binding constant Ka was calculated using the following equation [66]:

$$\text{Log} \left[(F_0/F)/F \right] = \text{Log} K_a + n \log [Q] \quad (6)$$

A plot of log $[(F_0/F)/F]$ versus log $[Q]$ gives a straight line. From the slope of the linear curve, we can obtain the value of the binding constant K_a.

G4.0-DOX fluorescence measurements were carried out for post-dialysis complexes with an initial G4.0-DOX molar ratio of 1:12 and 1:24 and an initial pH of 9.5. The exact methodology for preparing the complexes is described in our previous work [29]. Briefly, sufficient DOX at pH = 9.5 was added to the dendrimer at a constant concentration of 0.25 mg/mL (17.6 μM) and pH = 9.5 to give a molar ratio of the starting complexes of 1:12 and 1:24. The complexes were mixed for 24 hours and dialyzed using Slide-A-Lyzer™ Dialysis Cassettes (MWCO 10.0 kDa), Thermo Fisher (Waltham, MA, USA) for another 24hours to remove drug molecules not bound to the dendrimer. The final pH of the post-dialysis complexes stabilized at pH = 7.5. All fluorescence spectra were measured at an excitation of λ_{ex} = 482 nm and the emission was recorded between λ_{em} = 490 – 700 nm.

4.9. Isothermal Calorimetry (ITC) Measurements

ITC experiments were carried out using a Nano ITC calorimeter (TA Instruments) with a standard volume of 1.0 mL at 25 °C. All the solutions were prepared in deionized water (> 18Ω) and PBS buffer solution. All the solutions used to fill the cell and the syringe were degassed before analysis. The reference cell was filled with deionized water. The G4.0 PAMAM dendrimer was an analyte (0.0176mM) in the cell, and DOX (2.12mM) was a titrant in the syringe. Each time freshly prepared titrant solution was taken up in a 250 μL injection syringe and titrated into freshly G4.0 PAMAM solution. A total number of 25 (10 μL) or 50 injections (5 μL) were added after the calorimeter finalized the primary equilibration. The intervals between the injections were 200s and 300 s, respectively, leaving 200 s at the beginning of the experiment without injection. The stirring rate was set at 300 rpm. The control experiments to determine the heat of the dilution of DOX were performed by injecting the same concentration of DOX into the buffer. The calorimeter was operated using Nano ITC Run software, and all the data obtained were analyzed using the NanoAnalyze v. 3.1.2 program provided by the manufacturer. An 'independent' and 'multiple sites model' were used to evaluate the results. At least three independent measurements were collected, and ITC data and reproducible data were employed. For thermodynamic parameters calculation, a total number of 25 (10 μL) injections were used.

4.10. Release Studies

Release tests were performed for the G4.0-DOX complex at a molar ratio of 1:6 and pH = 9.5. The complex was prepared in accordance with a previously developed methodology [29]. The concentration of components in the final complex was $c_{G4.0}$= 250 μg/mL, c_{DOX}= 22 μg/mL (EE= 37.93%). The pH of the complex stabilized at pH=7.5. An aqueous solution of DOX with c=22 μg/mL and pH = 7.5 was prepared as a reference solution. Prepared G4.0-DOX complex and the reference DOX solution were placed in dialysis membranes (Thermo Scientific™ Slide-A-Lyzer™ MINI Dialysis Devices, MWCO 3.5 kDa). The dialysis bag was submerged in 45 cm^3 of Dulbecco's PBS buffer at pH 7.4, and was incubated at 25°C for 96 h. The released DOX in the incubation buffer was analyzed at predetermined time intervals using a Thermo Scientific Evolution 201 UV-vis spectrophotometer by measuring the spectrum in the wavelength range of λ = 190 – 800 nm. The concentration of released DOX was determined using the previously determined extinction coefficient $\varepsilon_{DOX\ pH\ 7.5}$ = 9610 M^{-1} cm^{-1} at λ_{max} = 480 nm [29]. Kinetic parameters were determined from the curves fitting and calculated using the equation:

$$y = a(1-e^{-bx}) \quad (7)$$

where:

y – DOX released [%]
x – time [h]
a – maximal amount of released DOX (A_{max}) [%]
b – release rate constant (k_1) [h^{-1}]

4.11. Cell Culture and Cytotoxicity of the Systems Against Malignant Cells

For the study, the following cell lines were used: colon cancer cell lines (HT-26, LoVo, and LoVoDX), lung cancer cell lines (NCI-H23 and H69AR), breast cancer cell lines (MCF-7 and MCF-7/DX), skin cancer cell line A375 and immortalized keratinocytes (HaCaT) as a model of the normal cell line. Cells were maintained at 37°C and 5% CO_2, colon cancer cells were maintained in a Ham's/F12 medium, and other lines in a Dulbecco's Modified Eagle's Medium (Sigma-Aldrich) supplemented with 10% fetal bovine serum (Fetal Bovine Serum, Heat Inactivated, non-USA origin, sterile-filtered, Sigma-Aldrich), and antibiotics: 100 IU/ml penicillin, and 0.1 mg/mL streptomycin (Gibco, Gaithersburg, MD, USA). For the experiments, cells were removed from culture flasks (Sarstedt, Warsaw, Poland) with a 0.25% trypsin-EDTA solution (IITD, Wroclaw, Poland), and suspended to a 96-well plate (Sarstedt) at a cell density 2 x 10^4/mL. Then, cells were maintained for 24 h in a CO_2 incubator for cell attachment. The next day, the plate medium was removed and 200 μL

of DOX/dendrimers/conjugates diluted with a culture medium was added to the appropriate wells for 24 and 72h. The final concentration of DOX conjugated with G4PAMAM dendrimers or unconjugated was 1, 2, 4 and 8 µM. Blank vehicle controls as equivalents of these concentrations were also examined. After the incubation cell viability was examined with the MTT assay, previously described in [67].

The absorbance was measured at 560 nm with the GloMax® Discover Microplate Reader (Promega). The results presented on the plots are blank-subtracted and normalized to the non-treated control. Cell viability values were represented as a percentage of the untreated control cells (100 %). Experiments were performed in triplicates. One-way ANOVA followed by Dunnett's multiple comparisons test was performed with the GraphPad Prism software, version 7.0. (GraphPad Software, San Diego). Dunnett's multiple comparisons test was chosen as it allows for comparing multiple treatment groups against a single control group, which aligns with our experimental design. Differences between treated samples and control cells with $p \leq 0.05$ were taken to be statistically significant.

4.12. Intracellular Distribution of Doxorubicin by CLSM Study

Two cell lines were used to distribute free and encapsulated DOX intracellularly: skin cancer cells -A375 and normal keratinocytes – HaCaT. Cells were trypsinized and placed on microscopic cover round glasses (Φ18 mm, Carl Roth GmbH, Germany) in 6-well plate (Equimed, Poland). Cells were seeded on a 96-well plate for intravital imaging. In both cases, cells were left for 24h to adhere and subsequently exposed to free DOX, DOX in nanocarriers, and empty nanocarriers for 24h or 72h. After that, cells were fixed by exposing it for 10 min to 4% paraformaldehyde (Polysciences, Inc., Bergstrasse, Germany) and washed in PBS (IITD, Wroclaw, Poland). FluorshieldTM with DAPI (4,6-diamidino-2-phenylindole) (Merck, Sigma-Aldrich, Poznan, Poland) was used to counterstain the nuclei and to mount the cells, and was excited by 405 nm-excitation channel. Intravital imaging was performed after 24h. The samples were studied on the MICA Microhub confocal microscopy (Leica Microsystems, CellService, Poznan, Poland).

5. Conclusions

To sum up, our studies illustrate that doxorubicin, which occurs in a protonated form in a physiological environment, becomes deprotonated at a higher pH. These are ideal conditions for forming a complex between positively charged G4.0 PAMAM dendrimers and negatively charged doxorubicin. It has been shown that at low concentrations of DOX in the absence of self-association, the drug forms an effective complex with the G4.0 PAMAM dendrimer. The conditions for the complex formation determine the drug's affinity, which depends on the pH and the degree of ionization of the components. The dendrimer endothermically binds doxorubicin at two binding sites - hydrophobic spaces and on charged surface groups. This is possible due to the properties of the DOX molecule and the presence of a hydrophobic anthraquinone in its structure, as well as functional groups susceptible to ionization and electrostatic interactions. This is important in the application context since the localization of the drug in the carrier structure determines both the release kinetics, which in the case of the G4.0-DOX nanosystem is pH-dependent and the *in vitro* activity. The observed increase in IC50 values with higher DOX loading ratios in the PAMAM-DOX complexes is attributable to the complex interplay between drug release dynamics, dendrimer saturation, steric hindrance, and aggregation effects. These factors collectively influence the bioavailability and cytotoxic potential of the DOX when complexed with PAMAM dendrimers. Moreover, the observed lower toxicity of the DOX-dendrimer complex after 24 hours highlights the benefits of controlled drug delivery systems in modulating drug release and improving selectivity. In conclusion, our results support the potential of dendrimer-based complexes to enhance the therapeutic window of DOX, providing a strategic advantage in cancer treatment by reducing toxicity to normal cells while maintaining efficacy against cancer cells.

References

1. Mouridsen HT. Anthracyclines in the Treatment of Early Breast Cancer. *Drugs*. **1993**;45(2):1-3. doi:10.2165/00003495-199300452-00002

2. Cai F, Luis MAF, Lin X, et al. Anthracycline-induced cardiotoxicity in the chemotherapy treatment of breast cancer: Preventive strategies and treatment. *Mol Clin Oncol*. **2019;**11(1):15-23. doi:10.3892/mco.2019.1854

3. Maruf A, Milewska M, Lalik A, Wandzik I. pH and Reduction Dual-Responsive Nanogels as Smart Nanocarriers to Resist Doxorubicin Aggregation. *Molecules*. **2022;**27(18):1-12. doi:10.3390/molecules27185983

4. Zhu L, Yang S, Qu X, et al. Fibril-shaped aggregates of doxorubicin with poly-l-lysine and its derivative. *Polym Chem*. **2014**;5(19):5700-5706. doi:10.1039/c4py00686k

5. Pyne A, Kundu S, Banerjee P, Sarkar N. Unveiling the Aggregation Behavior of Doxorubicin Hydrochloride in Aqueous Solution of 1-Octyl-3-methylimidazolium Chloride and the Effect of Bile Salt on These Aggregates: A Microscopic Study. *Langmuir*. **2018**;34(10):3296-3306. doi:10.1021/acs.langmuir.8b00029

6. Tasca E, Alba J, Galantini L, et al. The self-association equilibria of doxorubicin at high concentration and ionic strength characterized by fluorescence spectroscopy and molecular dynamics simulations. *Colloids Surfaces A Physicochem Eng Asp*. **2019**;577(June):517-522. doi:10.1016/j.colsurfa.2019.06.005

7. D'Angelo NA, Noronha MA, Câmara MCC, et al. Doxorubicin nanoformulations on therapy against cancer: An overview from the last 10 years. *Biomater Adv*. **2022**;133:112623. doi:10.1016/j.msec.2021.112623

8. Arshad R, Salman Arshad M, Rahdar A, et al. Nanomaterials as an advanced nano-tool for the Doxorubicin delivery/ Co-Delivery—A Comprehensive Review. *J Drug Deliv Sci Technol*. **2023**;8:104432. doi:10.1016/j.jddst.2023.104432

9. Robella M, Vaira M, Argenziano M, et al. Exploring the use of pegylated liposomal doxorubicin (Caelyx®) as pressurized intraperitoneal aerosol chemotherapy. *Front Pharmacol*. **2019**;10:1-6. doi:10.3389/fphar.2019.00669

10. Barenholz Y. Doxil® - The first FDA-approved nano-drug: Lessons learned. *J Control Release*. **2012**;160(2). doi:10.1016/j.jconrel.2012.03.020

11. Praça FSG, Marinho HS, Martins MBF, Gaspar R, Corvo ML, Medina WSG. Current aspects of breast cancer therapy and diagnosis based on a nanocarrier approach. *Nanostructures Cancer Ther*.**2017**:749-774. doi:10.1016/B978-0-323-46144-3.00027-1

12. Richardson PF. Nanotechnology Therapeutics in Oncology-Recent Developments and Future Outlook. *Elsevier* ; **2012**. Vol 47. 1st ed. doi:10.1016/B978-0-12-396492-2.00016-3

13. Zhao N, C Woodle M, Mixson AJ. Advances in Delivery Systems for Doxorubicin. *J Nanomed Nanotechnol*. **2018**;09(05):1-9. doi:10.4172/2157-7439.1000519

14. Iwamoto T. Clinical application of drug delivery systems in cancer chemotherapy: Review of the efficacy and side effects of approved drugs. *Biol Pharm Bull*. **2013**;36(5):715-718. doi:10.1248/bpb.b12-01102

15. de Araújo RV, da Silva Santos S, Ferreira EI, Giarolla J. New advances in general biomedical applications of PAMAM dendrimers. *Molecules*. **2018;**23(11):1-27. doi:10.3390/molecules23112849

16. Wang J, Li B, Qiu L, Qiao X, Yang H. Dendrimer-based drug delivery systems: history, challenges, and latest developments. *J Biol Eng*. **2022**;16(1):1-12. doi:10.1186/s13036-022-00298-5

17. Zhou LP, Li JW, Yu B, et al. The drug loading behavior of PAMAM dendrimer: Insights from experimental and simulation study. *Sci China Technol Sci*. **2023**;66(4):1129-1140. doi:10.1007/s11431-022-2178-8

18. Svenson S. Dendrimers as versatile platform in drug delivery applications. *Eur J Pharm Biopharm*. **2009**;71(3):445-462. doi:10.1016/j.ejpb.2008.09.023

19. Kheraldine H, Rachid O, Habib AM, Al Moustafa AE, Benter IF, Akhtar S. Emerging innate biological properties of nano-drug delivery systems: A focus on PAMAM dendrimers and their clinical potential. *Adv Drug Deliv Rev*. **2021**;178:113908. doi:10.1016/j.addr.2021.113908

20. Fox LJ, Richardson RM, Briscoe WH. PAMAM dendrimer - cell membrane interactions. *Adv Colloid Interface Sci*. **2018**;257:1-18. doi:10.1016/j.cis.2018.06.005

21. Szota M, Wolski P, Carucci C, et al. Effect of Ionization Degree of Poly (amidoamine) Dendrimer and 5-Fluorouracil on the Efficiency of Complex Formation — A Theoretical and Experimental Approach. *Int. J. Mol. Sci.* **2023**, *24*, 819. https://doi.org/10.3390/ijms24010819

22. Vidal F, Guzman L. Dendrimer nanocarriers drug action: Perspective for neuronal pharmacology. *Neural Regen Res*. **2015**;10(7):1029-1031. doi:10.4103/1673-5374.160063

23. Starpharma Ltd. About Starpharma. **2021**. https://www.starpharma.com/company (Access date: 12.03.2024)

24. Starpharma Ltd. Dendrimer Enhanced Product (DEP®) Drug Delivery. **2021.** https://www.starpharma.com/drug_delivery (Access date: 12.03.2024)

25. Kisakova LA, Apartsin EK, Nizolenko LF, Karpenko LI. Dendrimer-Mediated Delivery of DNA and RNA Vaccines. *Pharmaceutics*. **2023**;15(4). doi:10.3390/pharmaceutics15041106

26. Yoncheva K, Tzankov B, Yordanov Y, et al. Encapsulation of doxorubicin in chitosan-alginate nanoparticles improves its stability and cytotoxicity in resistant lymphoma L5178 MDR cells. *J Drug Deliv Sci Technol*. **2020;**59(July):101870. doi:10.1016/j.jddst.2020.101870

27. Bandak S, Ramu A, Barenholz Y, Gabizon A, Reduced UV-Induced degradation of Doxorubicin Encapsulated in Polyethyleneglycol-coated Liposomes, *Pharmaceutical Research*, **1999**, 16;9

28. Rai DB, Medicherla K, Pooja D, Kulhari H. Dendrimer-Mediated Delivery of Anticancer Drugs for Colon Cancer Treatment. *Pharmaceutics*. **2023**;15(3). doi:10.3390/pharmaceutics15030801

29. Szota M, Jachimska B. Effect of Alkaline Conditions on Forming an Effective G4.0 PAMAM Complex with Doxorubicin. *Pharmaceutics* **2023**, 15, 875. https://doi.org/10.3390/pharmaceutics15030875

30. Fülöp Z, Gref R, Loftsson T. A permeation method for detection of self-aggregation of doxorubicin in aqueous environment. *Int J Pharm*. **2013**;454(1):559-561. doi:10.1016/j.ijpharm.2013.06.058

31. Ryzhkina I, Murtazina L, Kostina L, et al. Doxorubicin aqueous systems at low concentrations: Interconnection between self-organization, fluorescent and physicochemical properties, and action on hydrobionts. *Front Chem*. **2022**;10(December):1-15. doi:10.3389/fchem.2022.1063278

32. Nguyen TN, Nguyen TT, Nghiem THL, et al. Optical properties of doxorubicin hydrochloride load and release on silica nanoparticle platform. *Molecules*. **2021**;26(13). doi:10.3390/molecules26133968

33. Changenet-Barret P, Gustavsson T, Markovitsi D, Manet I, Monti S. Unravelling molecular mechanisms in the fluorescence spectra of doxorubicin in aqueous solution by femtosecond fluorescence spectroscopy. *Phys Chem Chem Phys*. **2013**;15(8):2937-2944. doi:10.1039/c2cp44056c

34. Tasca E, D'Abramo M, Galantini L, et al. A Stereochemically Driven Supramolecular Polymerisation. *Chem - A Eur J*. **2018**;24(32):8195-8204. doi:10.1002/chem.201800644

35. Tokarczyk K, Jachimska B. Quantitative interpretation of PAMAM dendrimers adsorption on silica surface. *J Colloid Interface Sci*. **2017**;503:86-94. doi:10.1016/j.jcis.2017.05.002

36. Szota M, Reczyńska-Kolman K, Pamuła E, Michel O, Kulbacka J, Jachimska B. Poly(Amidoamine) dendrimers as nanocarriers for 5-fluorouracil: Effectiveness of complex formation and cytotoxicity studies. *Int J Mol Sci*. **2021**;22(20). doi:10.3390/ijms222011167

37. Yamada Y. Dimerization of Doxorubicin Causes Its Precipitation. *ACS Omega*. **2020**;5(51):33235-33241. doi:10.1021/acsomega.0c04925

38. Jachimska B, Tokarczyk K. Combining Surface Plasmon Resonance and Quartz Crystal Microbalance to Determine Hydration of Dendrimer Monolayers. *J Phys Chem C*. **2016**;120(35):19678-19685. doi:10.1021/acs.jpcc.6b05020

39. Ho MN, Bach LG, Nguyen TH, et al. PEGylated poly(amidoamine) dendrimers-based drug loading vehicles for delivering carboplatin in treatment of various cancerous cells. *J Nanoparticle Res*. **2019**;21(2). doi:10.1007/s11051-019-4486-5

40. Zheng X, Wang T, Jiang H, et al. Incorporation of Carvedilol into PAMAM-functionalized MWNTs as a sustained drug delivery system for enhanced dissolution and drug-loading capacity. *Asian J Pharm Sci*. **2013**;8(5):278-286. doi:10.1016/j.ajps.2013.09.001

41. Radu IC, Zaharia C, Hudiță A, et al. In vitro interaction of doxorubicin-loaded silk sericin nanocarriers with mcf-7 breast cancer cells leads to dna damage. *Polymers (Basel)*. **2021**;13(13). doi:10.3390/polym13132047

42. Kauffman M, Kauffman M, Zhu H, Jia Z, Li Y. Fluorescence-Based Assays for Measuring Doxorubicin in Biological Systems. *React Oxyg Species*. **2016**;2(6):432-439. doi:10.20455/ros.2016.873

43. Gjerde NS, Nardi AN, Chen CG, et al. Complexation and organization of doxorubicin on polystyrene sulfonate chains: impacts on doxorubicin dimerization and quenching. *Phys Chem Chem Phys*. **2022**;24(42):25990-25998. doi:10.1039/d2cp02714c

44. Chanphai P, Bekale L, Sanyakamdhorn S, et al. PAMAM dendrimers in drug delivery: Loading efficacy and polymer morphology. *Can J Chem*. **2017**;95(9):891-896. doi:10.1139/cjc-2017-0115

45. Saboury AA. A Review on the Ligand binding study by Isothermal Titration Calorimetry Iranian Chemical Society A Review on the Ligand Binding Studies by Isothermal Titration Calorimetry. *J Iran Chem Soc*. **2014**;3(1):1-21.

46. Olsson TSG, Ladbury JE, Pitt WR, Williams MA. Extent of enthalpy-entropy compensation in protein-ligand interactions. *Protein Sci*. **2011**;20(9):1607-1618. doi:10.1002/pro.692

47. Ross PD, Subramanian S. Thermodynamics of macromolecular association reactions: Analysis of forces contributing to stabilization. *Biophys J*. **1980**;32(1):79-81. doi:10.1016/S0006-3495(80)84918-6

48. Jachimska B, Łapczyńska M, Zapotoczny S. Reversible swelling process of sixth-generation poly(amido amine) dendrimers molecule as determined by quartz crystal microbalance technique. *J Phys Chem C*. **2013**;117(2):1136-1145. doi:10.1021/jp307832p

49. Singh V, Kesharwani P. Dendrimer as a promising nanocarrier for the delivery of doxorubicin as an anticancer therapeutics. *J Biomater Sci Polym Ed*. **2021**;32(14). doi:10.1080/09205063.2021.1938859

50.   Zhang M, Zhu J, Zheng Y, et al. Doxorubicin-conjugated PAMAM dendrimers for pH-responsive drug release and folic acid-targeted cancer therapy. *Pharmaceutics*. **2018**;10(3):1-13. doi:10.3390/pharmaceutics10030162

51.   Marcinkowska M, Sobierajska E, Stanczyk M, Janaszewska A, Chworos A, Klajnert-Maculewicz B. Conjugate of PAMAM dendrimer, doxorubicin and monoclonal antibody-trastuzumab: The new approach of a well-known strategy. *Polymers (Basel)*. **2018**;10(2):1-11. doi:10.3390/polym10020187

52.   Pessina A, Raimondi A, Cerri A, et al. High sensitivity of human epidermal keratinocytes (HaCaT) to topoisomerase inhibitors. *Cell Prolif*. **2001**;34(4):243-252. doi:10.1046/j.0960-7722.2001.00214.x

53.   Press D. Doxorubicin-conjugated dexamethasone induced MCF-7 apoptosis without entering the nucleus and able to overcome MDR-1-induced resistance. *Drug Des Devel Ther*. **2018**:2361-2369. doi: 10.2147/DDDT.S168588

54.   Olszówka M, Russo R, Mancini G, Cappelli C. A computational approach to the resonance Raman spectrum of doxorubicin in aqueous solution. *Theor Chem Acc*. **2016**;135(2):1-15. doi:10.1007/s00214-015-1781-9

55.   Rabbani A, Finn RM, Ausió J. The anthracycline antibiotics: Antitumor drugs that alter chromatin structure. *BioEssays*. **2005**;27(1):50-56. doi:10.1002/bies.20160

56.   Florêncio E Silva E, Machado ES, Vasconcelos IB, et al. Are the Absorption Spectra of Doxorubicin Properly Described by Considering Different Tautomers? *J Chem Inf Model*. **2020**;60(2):513-521. doi:10.1021/acs.jcim.9b00785

57.   Anand R, Ottani S, Manoli F, Manet I, Monti S. A close-up on doxorubicin binding to γ-cyclodextrin: An elucidating spectroscopic, photophysical and conformational study. *RSC Adv*. **2012**;2(6):2346-2357. doi:10.1039/c2ra01221a

58.   Papagiannaros A, Dimas K, Papaioannou GT, Demetzos C. Doxorubicin-PAMAM dendrimer complex attached to liposomes: Cytotoxic studies against human cancer cell lines. *Int J Pharm*. **2005**;302(1-2):29-38. doi:10.1016/j.ijpharm.2005.05.039

59.   Zhang C, Pan D, Luo K, et al. Dendrimer-doxorubicin conjugate as enzyme-sensitive and polymeric nanoscale drug delivery vehicle for ovarian cancer therapy. *Polym Chem*. **2014**;5(18):5227-5235. doi:10.1039/c4py00601a

60.   Guo W, Song Y, Song W, et al. Co-delivery of Doxorubicin and Curcumin with Polypeptide Nanocarrier for Synergistic Lymphoma Therapy. *Sci Rep*. **2020**;10(1). doi:10.1038/s41598-020-64828-1

61.   Nurcahyanti ADR, Wink M. L-Canavanine potentiates the cytotoxicity of doxorubicin and cisplatin in arginine deprived human cancer cells. *PeerJ*. **2016**;2016(1). doi:10.7717/peerj.1542

62.   Biswas A, Ghosh T, Gavel PK, Das AK. PEG Functionalized Stimuli Responsive Self-Healable Injectable Dynamic Imino-boronate G-quadruplex Hydrogel for the Delivery of Doxorubicin. *ACS Appl Bio Mater*. **2020**;3(2). doi:10.1021/acsabm.9b01034

63.   Liu SX, Kim JT. Application of Kevin—Voigt Model in Quantifying Whey Protein Adsorption on Polyethersulfone Using QCM-D. *J Lab Autom*. **2009**;14(4):213-220. doi:10.1016/j.jala.2009.01.003

64.   Komorek P, Martin E, Jachimska B. Adsorption and conformation behavior of lysozyme on a gold surface determined by qcm-d, mp-spr, and ftir. *Int J Mol Sci*. **2021**;22(3):1-17. doi:10.3390/ijms22031322

65.   Easley AD, Ma T, Eneh CI, Yun J, Thakur RM, Lutkenhaus JL. A practical guide to quartz crystal microbalance with dissipation monitoring of thin polymer films. *J Polym Sci*. **2022**;60(7):1090-1107. doi:10.1002/pol.20210324

66. Chinnathambi S, Velmurugan D, Hanagata N, Aruna PR, Ganesan S. Investigations on the interactions of 5-fluorouracil with bovine serum albumin: Optical spectroscopic and molecular modeling studies. *J Lumin*. **2014**;151:1-10. doi:10.1016/j.jlumin.2014.01.063

67. Kulbacka J, Kotulska M, Rembiałkowska N, et al. Cellular stress induced by photodynamic reaction with CoTPPS and MnTMPyPCl5 in combination with electroporation in human colon adenocarcinoma cell lines (LoVo and LoVoDX). *Cell Stress Chaperones*. **2013;**18(6):719-731. doi:10.1007/s12192-013-0423-1